11-2006

Submicrosecond Dynamics of Water Explosive Boiling and Lift-Off from Laser-Heated Silicon Surfaces

S. I. Kudryashov
Arkansas State University

S. D. Allen
Arkansas State University, allens17@erau.edu

Submicrosecond dynamics of water explosive boiling and lift-off from laser-heated silicon surfaces

S. I. Kudryashov[a] and S. D. Allen
Department of Chemistry and Physics, Arkansas State University, Jonesboro, Arkansas 72467-0419

(Received 3 June 2006; accepted 29 August 2006; published online 28 November 2006)

Explosive boiling and lift-off of a thin layer of micron-sized transparent water droplets from an absorbing Si substrate heated by a nanosecond KrF laser were studied using a contact photoacoustic technique. The compressive photoacoustic response increases steeply to an asymptotic value on the order of the water critical pressure starting at a threshold laser fluence of 0.20 J/cm^2, where lift-off of the water layer also occurs. Above this threshold, several reproducible discrete multimegahertz components are revealed in Fourier spectra of the acoustic transients, corresponding to nanosecond oscillations of steam bubbles inside the water droplets on the microsecond time scale of the lift-off process. The acoustic pressure buildup, bubble dynamics, and the subsequent lift-off of the thin water layer are interpreted as relaxation stages after near-spinodal explosive boiling of the superheated interfacial water. © *2006 American Institute of Physics*. [DOI: 10.1063/1.2372317]

I. INTRODUCTION

Microscopic behavior of cavitating liquids at high thermal loads (heat flux density per unit surface) at solid/liquid interfaces is very important for robust cooling of nuclear reactors,[1] steam laser cleaning of contaminating particulates from critical solid surfaces,[2] and precision control of laser-induced forward transfer of nano- and micropatterns.[3] It is known that increase of thermal load at the solid/liquid interface results in transition from a "convection" regime to a "nucleate boiling" regime and, after the Leidenfrost point, to a "film boiling" regime, representing increasing superheating of the solid surface relative to normal (spontaneous) boiling temperature of the liquid at atmospheric pressure, $\Delta T = T - T_{spon}(P=1\ \text{atm})$.[4] In the "transition" regime between the two stable boiling regimes the surface temperature as well as ΔT suddenly rises to much higher values as a response to transformation of separate interfacial vapor bubbles at the solid surface to a continuous interfacial insulating vapor layer, with the final solid surface temperature strongly dependent on the magnitude of the thermal load applied. In particular, on nanosecond or shorter time heating scales, such non-steady-state liquid/vapor transformation at positive external pressures (sometimes called explosive boiling) at liquid/solid interfaces can be realized in superheated liquids via quasihomogeneous nucleation of tiny vapor bubbles near corresponding liquid/vapor spinode curves,[5] where the "critical" bubble radius $r \to 0$ at $T \to T_{spin}$ with T_{spin} denoting the pressure-dependent temperature of a spinodal liquid/vapor transition. Although this phenomenon is widely used in steam laser cleaning and laser-induced forward transfer applications,[2,3] it could be a factor of risk in cooling cycles of industrial processes, as violent cavitation of cooling liquids in the transition regime frequently accompanied in the bubble collapse phase by intense short-wavelength sonoluminescence[6] and emission of shock waves[7] may cause enhanced microscopic cavitation damage of solid surfaces,[8] reducing their cooling capacity. These and other microscopic processes underlying explosive boiling of liquids at hot solid surfaces and involving dynamics of multiple interfacial vapor bubbles in steam laser cleaning, laser-induced forward transfer, and cooling applications are not yet well understood.[1–8] Importantly, explosive boiling and all of the above mentioned accompanying phenomena may occur differently when scaled down to micrometer size, e.g., when realized in microheaters or in cooling cycles of microsystems.[1]

Interfacial explosive boiling has been the subject of intense experimental and theoretical studies over the last few decades.[1–6,8–21] Historically, such experiments using optical reflectance,[9,10] scattering,[10] transmission,[11] interferometric[12] and beam deflection[13,14] techniques, as well as photoacoustics[14,15] were started on atomically rough surfaces of Cr or Ag thin metallic films immersed in bulk low-boiling organic liquids (or water) and heated by pulsed nanosecond laser radiation. As a result, submicrosecond bubble nucleation has been observed at very moderate boiling parameters—degree of superheating $\Delta T \approx 20-100$ K (Refs. 9 and 10) for $T_{spon} \approx (0.7-0.8)T_{crit}$ (T_{crit} stands for the corresponding critical point temperature), pressures $P \approx 1-3$ MPa,[14,15] and bubble growth rates $U \approx 1-3.6$ m/s.[10,12,15] Later it was demonstrated that these results could be related to relative slow spontaneous heterogeneous nucleation and growth of interfacial vapor bubbles ("nucleate boiling"[4]) which can be suppressed by applying moderate hydrostatic pressures (e.g., $P=3$ MPa for water[9]) which are much lower than the saturated vapor pressure for these liquids at minimal $T_{spin}(P>0) \approx 0.9T_{crit}$.[5] At atmospheric pressure and high laser fluences heating the metallic substrates, heterogeneous vapor bubbles were observed to coalesce to a continuous nearly flat interfacial vapor layer ("film boiling" mechanism[4]) which continuously grows and makes a large final bubble, but then splits back to separate bubbles sometime during subsequent submicrosecond relaxation.[12] In con-

[a]Author to whom correspondence should be addressed; electronic mails: skudryashov@astate.edu and sergeikudryashov@yahoo.com

trast, much smaller heterogeneous final bubbles nucleated on micron-sized heated spots—surfaces of microheater[1] or micron-wide coating of an optical fiber tip,[16] demonstrated long-term oscillation dynamics preceded by microsecond coalescence dynamics of smaller precursor bubbles.[16]

Principally different results have been obtained in explosive boiling studies on atomically smooth surfaces of commercial silicon (Si) wafers. For this type of surfaces onset of explosive boiling in superheated nanometer-thick interfacial water sublayers occurs at much higher laser fluences corresponding to temperatures, $T_{spon} \approx 520\ \mathrm{K} \geqslant 0.8T_{crit}$ (Ref. 17) [in bulk water at $T_{spon} \approx 563$ K (Refs. 5 and 8) $\leqslant 0.9T_{crit}$ for $T_{crit}=647$ K], i.e., in proximity of the liquid/vapor spinode of water.[5] Micron-thick and thinner liquid layers of low-boiling liquids transparent to pulsed nanosecond laser radiation heating Si wafer substrates were observed to explosively boil during the laser pulse in such superheated interfacial liquid sublayers above a certain threshold laser fluence F_B.[17–21] Bubble nucleation, growth, and coalescence within such superheated sublayer occur on a subnanosecond time scale converting it to an expanding two-dimensional nanometer-thick interfacial vapor sub-layer.[21] On a similar time scale the explosive boiling process builds up a multimegapascal interfacial pressure in the superheated nanometer-thick interfacial liquid sublayer,[20] which finally lifts off the entire liquid layer at a speed of tens of m/s,[18,19,21] inversely proportional to layer thickness[19] and decreasing versus laser fluence F as a function of the difference $(F-F_B)$.[18–21] Such high lift-off velocities of liquid layers on smooth Si surfaces—much higher than growth rates of heterogeneous bubbles at rough metallic interfaces[10,12,15]—require expansion rates in corresponding superheated nanometer-thick interfacial liquid sublayers approaching the speed of sound in these liquids, as shown from momentum conservation principles.[18–20] Importantly, these experimental findings are qualitatively supported by results of molecular dynamics (MD) simulations[22,23] demonstrating explosive boiling, pressure buildup, and lift-off processes at a nanoscale level corresponding to liquid/vapor transformation at the near-spinodal conditions. However, there are not yet much experimental data and understanding of microscopic—nano- and microscale—processes involving explosive boiling and subsequent transport phenomena, especially, in the final microheterogeneous liquid/vapor systems, which are of great interest for the fundamental theory of boiling phenomena and various applications. Unfortunately, the common optical reflection,[9,10] scattering,[10,21] transmission[11] and interferometric[12,21] probes, and imaging techniques[24] (except x-ray based ones[25]) cannot be efficiently used in experimental studies of multiple light-scattering, short-lived mass density fluctuations in superheated liquids at spatial scales close or below the optical diffraction limit. Potentially, contact broadband photoacoustic spectroscopy, which has been employed for studies of short-term cavitation in bulk superheated liquids,[26] can also give insight into nano- and microscale boiling processes at solid/liquid interfaces, but characteristic cavitation effects—bubble oscillations and coalescence—have not been observed so far for the latter case.[14,15,20]

In this work we report a photoacoustic study of explosive boiling and lift-off of a predeposited layer of separate transparent micron-sized water droplets from an absorbing Si wafer heated by a nanosecond KrF laser. The laser-generated acoustic transients were recorded on a rear side of the Si wafer in a contact mode both for "wet" and reference dry Si surfaces. The rapid increase of the acoustic response at a threshold laser fluence, F_B, of 0.20 J/cm^2 and its subsequent leveling off at a value of order of the water critical pressure in the fluence range of 0.2–0.4 J/cm^2 are attributed to explosive boiling of superheated water driven by the strong nonlinearity of the water thermal expansion coefficient near the liquid-vapor spinode curve. Moreover, above F_B the recorded acoustic transients from "wet" Si surfaces contained several characteristic high-frequency (multimegahertz) contributions from spatially separated micron-sized steam bubbles with microsecond lifetimes nucleated in separate multimicron transparent water droplets. The photoacoustic studies of thresholdlike fast buildup of acoustic pressure and steam bubble dynamics at fluences above F_B give insight into preceding microscopic steps of explosive nucleation of steam nanobubbles and their coalescence to microbubbles in the host water droplets, growth of these microbubbles followed by the onset of hydrodynamic microflows inside the droplets and their final lift-off.

II. EXPERIMENTAL SETUP

A liquid dosing system described elsewhere[18–20] consists of a source of pressurized nitrogen with a triggered valve, connected to a bubbler immersed in a glass flask filled with heated de-ionized water and directed through a heated output nozzle onto a surface of 0.25 mm thick commercial Si(100) wafers (Motorola) mounted onto a three-dimensional stage at a distance of 5 cm from the nozzle. The dosing system (gas pressure of 0.7 bar, flask water and nozzle temperatures of 40 °C, and dosing times $\tau_{dose}=0.1-1.0$ s) was employed to deposit 3–6 cm wide (depending on τ_{dose}) layers of separate water droplets onto the Si wafers.

Deposition, laser removal, and natural drying of the water layers were monitored in real time both by time-resolved optical microscopy (Fig. 1) and by observing the optical reflectance/scattering of a helium-neon (HeNe) probe laser focused on the center of the dosed area (Fig. 2). Time-resolved optical microscopy visualization of the transient water droplets on the Si wafer surfaces was performed at a magnification of 400× under a Mitutoyo wide field-high eyepoint microscope equipped with a digital camera (Olympus 3030). Subsequent frames of water-dosed Si surfaces were taken at a rate of 30 frames/s and then these movies were analyzed using Windows Movie Maker graphics software to track spatiotemporal evolution of separate water droplets frame by frame. It was observed that at the instant t_{las} when the KrF laser fires the deposited water layer consists of separate micron-sized droplets [Fig. 1(b)] as the several nanometer-thick native silicon oxide surface film on the Si wafers has dewetting properties relative to water with an expected contact angle of 20°–45°.[27] Coalescence and Ostwald ripening of water droplets were found to occur on a multimillisecond time scale during and after the dosing

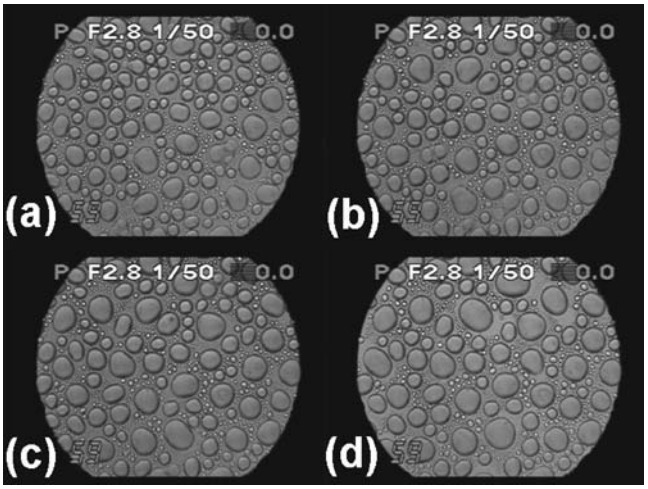

FIG. 1. Snapshots of the wet Si substrate for $\tau_{dose}=0.3$ s at $t=t_{las}$—33 ms (a), t_{las} (b), $t_{las}+33$ ms (c), and $t_{las}+100$ ms (d) (frame size 0.37 $\times 0.37$ mm^2). The KrF laser has not been fired in this series.

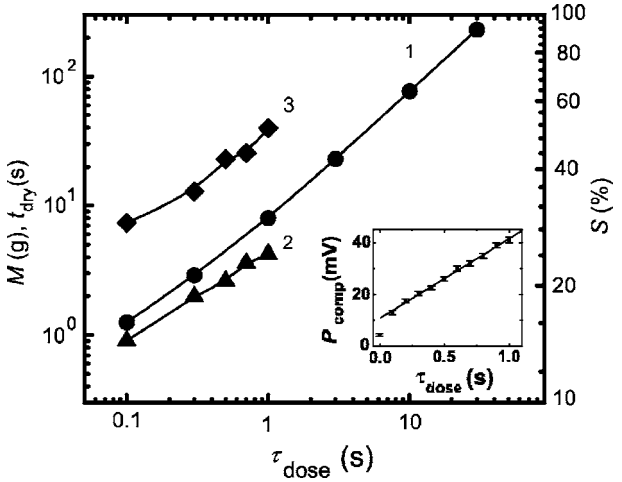

FIG. 3. Deposited water mass M (curve 1), drying time t_{dry} (curve 2), and Si surface coverage S (curve 3) as a function of τ_{dose}. Inset: compressive pressure P_{comp} for the wet Si substrate vs τ_{dose} at $F=2.3$ J/cm^2.

pulses [Figs. 1(c) and 1(d)], thus, being negligibly slow in the microsecond time frame of photoacoustic measurements performed in this work. Importantly, at t_{las} surface coverage, S, of the Si wafers by water droplets, i.e., the total surface of the water/Si boundary, was nearly linearly proportional to τ_{dose} within the range of 0.1–1.0 s (Fig. 3), indicating about constant thickness of large water droplets, $H\approx 7-10$ μm, at different τ_{dose}. This fact is consistent with the results of absolute measurements of deposited water mass, M, performed with $CaSO_4$ absorbent (drierite), exhibiting a linear increase of M with increasing τ_{dose} at the overall deposition rate of 0.007 g/s. A similar linear trend has been obtained for natural drying times, t_{dry}, vs τ_{dose} (Fig. 3) measured by tracking reflection/scattering of the probe HeNe laser from the water-dosed Si surfaces (Fig. 2), demonstrating local natural drying of the deposited water at the almost constant vaporization rate. The linear change of t_{dry} vs τ_{dose} can be interpreted in terms of the constant droplet thickness H, while the maximum total surface of the water/air boundary, being approximately equal to S for multimicron-sized droplets with their lateral widths $W \gg H$, linearly increases with τ_{dose}. Most probably, during the coalescence/Ostwald ripening and reverse natural drying process the water droplets are adjusting their

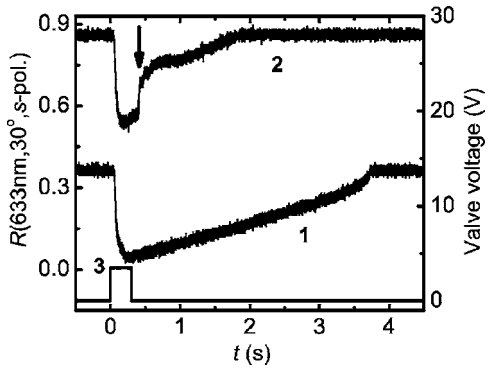

FIG. 2. Transients of HeNe laser reflectance/scattering from the water-dosed Si substrate with (1) and without (2) excimer laser shot and the corresponding 0.3 s electrical pulse for the dosing valve (3).

shapes (mainly, widths W of their top and bottom bases) to keep the droplet thickness constant for the reason of contact angle constraints for this combination of air/water/Si surfaces.

In the photoacoustic experiments the Si wafer was heated using a 248 nm, 20 ns [full width at half maximum (FWHM)] KrF excimer laser (Lambda Physik, LPX 210) described elsewhere.[18–20] The beam was apertured in its central part by a 1 cm wide vertical slit and was focused by a cylindrical lens ($f=10$ cm) at normal incidence in the center of the predeposited layer of water droplets. The laser beam has nearly rectangular and Gaussian fluence, F, distributions in the horizontal (X) and vertical (Y) directions with characteristic dimensions of $x=4$ and $\sigma_y=1.1$ mm, respectively. Laser energy [0.2 J/pulse (±3%) after the aperture] was attenuated by color filters (Corning Glass Works) and was measured by splitting off a part of the beam to a pyroelectric detector (Gentec ED-500). The excimer laser was fired 0.06 s after the end of each deposition step, accounting for the approximately 40 ms delay for the dosing nitrogen pulse to propagate inside the dosing system between the gas valve and the Si substrate surface. This laser and the gas valve of the dosing system were triggered manually in a single-shot mode with the corresponding delays generated using a pulse generator (Stanford Research Systems DG 535).

During the photoacoustic measurements the Si wafer was attached to the front surface of a fast 1.5 mm thick, 8 mm wide acoustic transducer [lead zirconate titanate (PZT) ceramic, effective bandwidth of 3–10 MHz, with a protective brass disk of thickness $D=3$ mm) by means of a thin vacuum grease layer providing acoustic contact between the wafer and transducer.[20,28] A LeCroy 9360 storage oscilloscope (50 Ω inputs) triggered by a fast Si photodiode, detecting a part of the excimer laser beam scattered from the entrance slit, was employed simultaneously to measure the laser pulse energy using the same calibrated photodiode and to record the acoustic transients within the operating time window of the acoustic transducer (the first 300 ns). Longer acoustic transients recorded in this work included acoustic

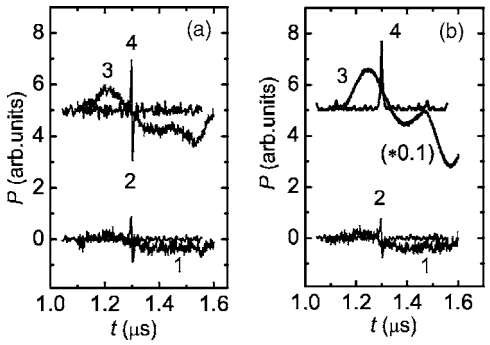

FIG. 4. (a) Acoustic transients for the dry Si substrate at $F=0.16$ J/cm^2 $\leqslant F_B$ (1), $F=0.38$ J/cm^2 $\geqslant F_B$ (3), and the corresponding reconstructed wave forms (2,4, not to scale); (b) acoustic transients for the wet Si substrate at the same fluences (1,3) and their reconstructed wave forms (2,4, not to scale). The transients are offset for clarity.

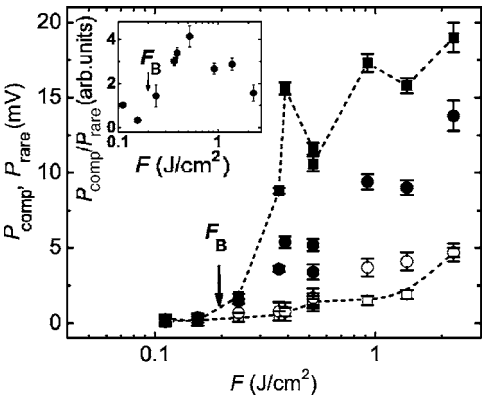

FIG. 5. Pressure amplitudes P_{comp} (squares) and P_{rare} (circles) vs F for the dry (open symbols) and wet (solid symbols) Si substrates. Inset: P_{comp}/P_{rare} ratio for the wet Si substrate as a function of F.

reverberations in the acoustic detection system. All these transients were delayed by 1.15 μs mostly due to the protective brass disk. Measurements were performed at laser fluences $F=0.1-2.4$ J/cm^2 both for dry and wet (dosed with water for $\tau_{dose}=0.3$ s) Si surfaces, with the former (dry) case providing a reference signal as the acoustic source is localized into the Si wafer. At $\tau_{dose}=0.3$ s characteristic widths W and thicknesses H of water droplets in Fig. 1 are 10–30 and 7–10 μm, respectively. Importantly, in agreement with the above mentioned studies of water dosing conditions, a compressive photoacoustic response, P_{comp}, for wet Si surfaces increases linearly with increasing τ_{dose} (Fig. 3, inset) at laser fluences above the corresponding explosive boiling threshold, $F_B \approx 0.2$ J/cm^2, for water droplets on Si surface.[18]

III. RESULTS AND INTERPRETATION

A. Experimental photoacoustic results

Characteristic recorded bipolar photoacoustic transients are presented in Figs. 4(a) and 4(b) for dry and wet Si surfaces and two fluence ranges, $F<F_B$ and $F>F_B$, where significant changes in temporal profiles and amplitudes of the transients occur near the threshold value $F_B=0.20\pm0.04$ J/cm^2. This boiling threshold F_B for water is consistent with that of 0.08 J/cm^2, reported[17] for explosive boiling of water on atomically smooth Si surfaces at the 532 nm laser wavelength and much shorter 8 ns pulse width τ_{las}. For higher Si reflectivity R of 0.6 at 248 nm vs 0.4 at 532 nm calculated using tabulated optical constants of Si,[29] and different laser pulse widths, $\tau_{las}(\text{FWHM}) \approx 20$ ns in this work versus $\tau_{las}(\text{FWHM}) \approx 8$ ns reported,[17] laser-induced deposition of the same volume energy density $\Theta \approx (1-R)F/(\chi^S \tau_{las})$ (Ref. 30) in Si affected by heat conduction with the thermal diffusivity χ^S requires 2.5 times higher laser fluence at 248 nm as compared to 532 nm, which is exactly the case in this work (0.20 J/cm^2 vs 0.08 J/cm^2).

At $F<F_B$ these photoacoustic transients exhibit identical, nearly symmetrical bipolar wave forms for dry and wet Si surfaces [Fig. 4(a) and 4(b)], characteristic of a linear thermoacoustic response, $P(t) \propto (dI_{las}/dt')_{t'=t}$,[30] from the acoustically free water/Si and dry Si boundaries, where $I_{las}(t)$ represents the temporal intensity profile of the laser pulse. In this case, the first positive pulse corresponds to compressive pressure, P_{comp}, resulting from thermal expansion of the laser-heated near-surface layers of water and, predominantly, Si, and the second negative pulse corresponds to tensile pressure, P_{rare}, in the layers because of their contraction during the cooling process at the end of the laser pulse.[20,30]

In contrast, at $F>F_B$ [Fig. 4(a) and 4(b)] photoacoustic transients obtained for the water/Si boundary start to exhibit much higher amplitudes relative to those from the dry Si surface and strongly asymmetric wave form shapes with the compression amplitude dominant. Moreover, at fluences above F_B visual lift-off of the deposited water layers appears in the form of a several millimeter-long water plume consisting of a vapor/droplet mixture.[18] In accordance with the results of temperature calculations presented in Sec. III B, and results of previous photoacoustic studies for continuous liquid layers or bulk liquids[14,15,20] as well as with the following discussion in Sec. IV, these data represent a nonlinear thermoacoustic response, $P(t) \propto I_{las}(t)$,[30] of the superheated interfacial water layers in each droplet irradiated at $F>F_B$, as a result of explosive boiling of these layers. Note that there is a nearly two times increase of pressure amplitudes for acoustic waves transmitted from water into a bulk Si for the pressure transmittance of the water/Si boundary, $\Im_{water/Si}=2/(N+1)$,[31] where $N=[\rho^L(T)C_l^L(T)]/[\rho^S C_l^S]$ is the impedance ratio for water and solid Si for their transient temperature-dependent mass densities, $\rho^L(T)$ and ρ^S, and longitudinal sound velocities, $C_l^L(T)$ and C_l^S, respectively [at normal conditions $N \approx 0.07$ and $\Im_{water/Si} \approx 2$ for $\rho^L(300\text{ K}) \approx 1.0$ g/cm^3 and $\rho^S \approx 2.33$ g/cm^3, $C_l^L(300\text{ K}) \approx 1.5$ km/s and $C_l^S \approx 8.8$ km/s (Ref. 32)] Subtracting the negligible contribution of the "dry" component (<5% at $F>F_B$) (Fig. 5) and accounting for partial coverage of the Si surfaces by water droplets, $S \approx 35\%$ at $\tau_{dose}=0.3$ s (Fig. 3), the actual value of the "water" compressive pressure, P^L, can be calculated as a function of F (Fig. 6), in good approximation, dividing P_{comp} by the corresponding factors $\Im_{water/Si}$ and S (see inset in Fig. 3 for coverage dependence).

Importantly, for all laser fluences used in this work, both with and without a water layer, significant broadening of the photoacoustic wave forms by nearly five times compared to the KrF laser pulse length $\tau_{las}(\text{FWHM}) \approx 20$ ns and de-

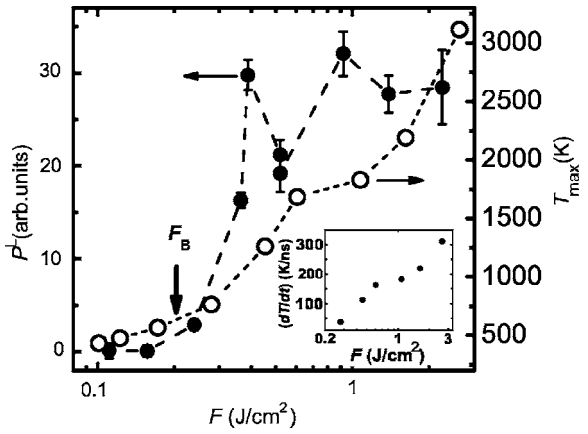

FIG. 6. Compressive pressure P^L as a function of F (left axis); dependence of maximum water/Si interface temperature T_{max} on F (right axis). Inset: laser heating rate (dT/dt) calculated for the water/Si interface at $T \approx 620$ K as a function of F.

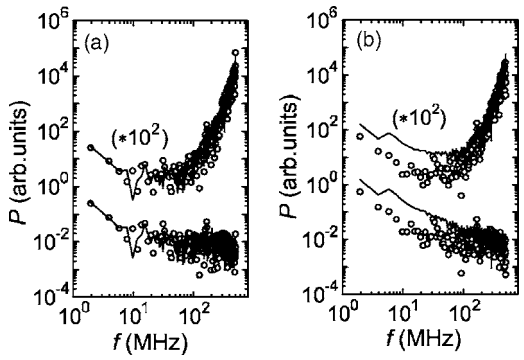

FIG. 7. Initial (bottom) and renormalized (top) amplitude FFT spectra of acoustic transients for dry (circles) and wet (line) Si substrates at $F \approx 0.16$ J/cm$^2 < F_B$ (a) and $F \approx 0.38$ J/cm$^2 > F_B$ (b) (offset for clarity). Spectral components in the range of 1–6 MHz are intrinsic features of the acoustic detection system.

creased amplitudes were observed (Fig. 4). These effects are largely attributable to dissipative losses for multimegahertz frequency components of the initial photoacoustic transients in the 3 mm thick protective brass disk and to reflections at all interfaces in the acoustic delay line. Additional losses in the very thin layers of vacuum grease and epoxy glue fixing the Si wafer and PZT element, respectively, in the acoustic transducer have only a minor effect. Moreover, the protective brass disk is thick enough to result in observable diffraction of the detected 100 ns (FWHM) acoustic pulses, which is revealed by the ratio of P_{comp} and P_{rare} values (Fig. 5, inset). Indeed, the acoustic pulse has a nearly plane wave front in the near acoustic field $(D/Z_{diffr} \approx 0.2)$ due to the wide laser spot on the Si wafer surface in our photoacoustic measurements, where the characteristic diffraction length equals $Z_{diffr} \approx \pi x \sigma_y / 2\lambda_{ac} \approx 15$ mm and the characteristic wavelength, λ_{ac}, of the 100 ns (FWHM) detected acoustic pulses for the brass longitudinal sound velocity $C_l^{brass} \approx 4.4 \times 10^3$ m/s (Ref. 32) is equal to about 0.5 mm. At $D/Z_{diffr} \approx 0.2$, the expected P_{comp}/P_{rare} ratio in the near acoustic field should be about 0.7 for bipolar symmetrical acoustic pulses and 3–3.5 for unipolar symmetrical compressive acoustic pulses,[20,30] respectively. In the latter case the diffraction effect results in 30% reduction of the P_{comp} amplitude and in the appearance of a spurious rarefaction pulse with an amplitude of nearly 25% from the initial P_{comp} value.[30] These expectations are consistent with our experimental observations in the inset in Fig. 5, exhibiting, on average, $P_{comp}/P_{rare} \approx 0.7 \pm 0.3$ at $F < 0.24$ J/cm^2 and 3.0 ± 0.2 at $F = 0.4$–1.4 J/cm^2 (excluding the data point at 2.4 J/cm^2, where laser ablation of Si takes place[28]). The drastic quantitative change of the P_{comp}/P_{rare} ratio for the acoustic response of water-dosed Si surfaces near F_B means a transition from acoustic generation at the free water/ boundary to that at the water/ boundary dynamically constrained by the water droplets. In other words, at $F > F_B$ the explosively boiling interfacial water layer in each water droplet on the Si surface is inertially confined during the acoustic relaxation (round-trip) time in the droplets, $t_{RT} \sim H/C_l^L$, which is on a order of a few nanoseconds, i.e., the explosive boiling process occurs faster than a the acoustic relaxation, in agreement with previous photoacoustic measurements for thin continuous liquid layers of 2-propanol.[20] Together with the explosive boiling effect, the diffraction effect provides the a rapid increase of P^L at $F \geq F_B$ and its following saturation at higher fluences (Fig. 6), indicating, potentially, thermal isolation of water droplets from the hot Si interface by the interfacial vapor layer.[4]

Additionally, reconstruction of the initial photoacoustic transients obtained for wet Si surfaces at $F < F_B$ and $F > F_B$ can be performed by multiplying Fourier spectra for pressure amplitude $P(f)$ (Fig. 7) obtained for the transients shown in Fig. 4 using a fast Fourier transform (FFT) option of Origin 7 (OriginLab Co.), by corresponding frequency-dependent pressure transmission coefficients for the brass disk $(D=3$ mm), $\Im_{brass}(f) \propto \exp\{-\alpha_{ac}(f)D\}$, taking the normalized absorption coefficient of sound $\alpha_{ac}/f = 7 \times 10^{-6}$ s/m at $f \sim 10$ MHz.[32] The resulting reconstructed transients presented in Fig. 4 show the reasonably correct, laser pulse-limited wave forms of acoustic transients, as expected from the general thermoacoustic theory.[30] Surprisingly, even though multimegahertz components are predominant in the renormalized frequency Fourier spectra of the photoacoustic transients at $F < F_B$ and $F > F_B$ (Fig. 7), contributing more strongly to the acoustic pressure P, in the "wet" Si case all frequencies in the range $f = 2$–200 MHz exhibit a similar steep fluence dependence near the threshold F_B [see in Fig. 8 $P_f^L(F)$ curves scaled by factors $\Im_{water/Si}$, $\Im_{brass}(f)$, and S]. The predominance of high-frequency ($f \geq 500$ MHz) components in the renormalized FFT spectra in Fig. 7 means that at $F > F_B$ the pressure buildup shown in Figs. 4–6 appears rapidly—on a time scale shorter than $1/f \approx 2$ ns (Ref. 20) during the 20 ns heating KrF laser pulse.

An insight into the origin of the impulsive pressure buildup comes from the Fourier analysis of longer acoustic transients for dry and wet Si surfaces at $F > F_B$. For wet Si they show the presence in the FFT spectra of a number of distinct spectral lines at $F > F_B$ (Fig. 9), which can be associated with steam bubble oscillations.[16,26] The bubble oscillations occur in the frequency range $f = 10$–35 MHz (as well as under near-spinodal conditions in superheated bulk

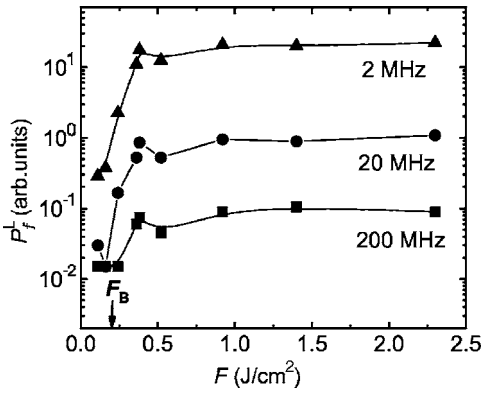

FIG. 8. P_f^L amplitudes scaled by factors $\Im_{water/Si}, \Im_{brass}(f)$ and S, vs F for f =2, 20, and 200 MHz.

water[26]), including the fundamental frequency $f_0 \approx 11.1 \pm 0.4$ MHz and its higher—second and third—harmonics mf_0 at 20.7 ± 0.4 and 33–34 MHz, respectively. Surprisingly, the initial phases of these oscillations are shifted with respect to each other by $\Delta\phi = 130° \pm 30°$ ($120° \pm 30°$ and $140° \pm 30°$), rather than in phase ($\Delta\phi = 0°$), indicating the additivity of the phases and, thus, supporting our interpretation of the oscillations in terms of higher harmonics. The bubble lifetimes, $\tau_{bub} = 1/\Gamma$ for the FWHM parameter $\Gamma \approx 0.8$ MHz of these spectral lines, are close to 1 μs, which is consistent with the fact that the corresponding bubble oscillations are only present in the FFT spectra obtained for time intervals lasting approximately τ_{bub} after the heating laser pulse. Microsecond lifetimes of the corresponding bubbles can be associated with the microsecond duration of the lift-off process for water droplets at $F > F_B$, driven by expansion of the interfacial steam bubbles and dictated by lift-off velocities of micron-thick water droplets which are on the order of a few m/s.[18]

B. Calculations of interfacial temperatures

To provide more firm interpretation of the experimental photoacoustic results, the maximum water/Si interface temperature, T_{max}, and its transient values have been calculated as a function of F using the computer code "SLIM" (Ref. 33) to solve a non-steady-state thermal conduction equation with temperature-dependent solid Si parameters (see calculation details elsewhere[20,28]). It has been shown[20,28] that such calculations give correct values of the Si surface temperatures for the onset of Si melting and ablation (melting temperature $T_m = 1689$ K, normal boiling temperature $T_{boil} \approx 3.6 \times 10^3$ K)[32] consistent with the experimentally observed acoustic responses of dry Si for melting (~ 0.5 J/cm^2) (Ref. 28) and ablation (~ 1.4 J/cm^2) (Ref. 28) thresholds. In this work, thermal fluxes in water and solid Si near the interface have been accounted for in the temperature calculations for a dry Si surface in the temperature range of 300–643 K, multiplying F in the "wet" Si case by the factor of $(1+\varepsilon S)$, calculated for the Si surface coverage by water droplets, S, and the ratio of the thermal fluxes, ε, or, similarly, the ratio of corresponding products $C_p^{L,S}(\chi^{LS})1/2$,[30] where $C_p^{L,S}$ and $\chi^{L,S}$ are the isobaric heat capacities and thermal diffusivities of water and Si, respectively. For water the ε value changes by about 15% from the mean value of 0.08 in the broad temperature range of 300–643 K nearly up to the critical temperature of water, $T_{crit} = 647$ K, as $C_p^L(T) \approx 4.2$ J/cm^3, $C_p^S(T) \approx 2$ J/cm^3, $\chi^L(T) \approx 1.5 \times 10^{-3}$ cm^2/s and $\chi^S(T) \approx 0.3$–0.7 cm^2/s do not change much at these temperatures.[5,32] Multiplying F in the "wet" Si case by the factor $(1+\varepsilon S)$ yields a new fluence scale, i.e., the same maximum interface temperature achieved at F in the dry Si case requires $(1+\varepsilon S)F$ in the "wet" Si case, while transient interface temperatures or heating rate (dT/dt) for the "wet" Si surface can be ascribed to higher fluences $(1+\varepsilon S)F$ in the same way. This scaling procedure is strictly applicable only for $F \leqslant F_B$, while at higher laser fluences boiling kinetics and non-steady-state, strongly reduced heat conduction in the interfacial boiling layer at the water/Si interface[4] rather than corresponding heat conduction of homogeneous liquid water should be considered in calculations of T_{max} vs F.

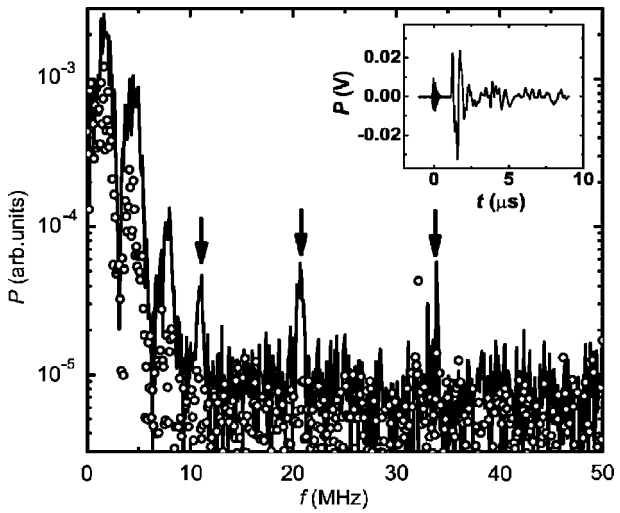

FIG. 9. Amplitude FFT spectra of acoustic transients at $F \approx 2.3$ J/cm^2 for dry (open circles) and wet (solid line) Si substrates. Inset: acoustic transient for "wet" Si at $F \approx 2.3$ J/cm^2.

The resulting dependence of $T_{max}(F)$, calculated for the case of the laser-heated water/Si interface, exhibits at $F \approx F_B$ near-spinodal temperatures $T_{max} \geqslant 0.95 T_{crit}$ (Fig. 6), consistent with previous calculations for thin continuous 2-propanol layers on Si substrates.[20] These temperature calculations support our photoacoustic observations of fast acoustic pressure buildup at $F \geqslant F_B$ and its interpretation as a phenomenon associated with nonlinear thermal expansion of the superheated interfacial water layer in the water droplets and consequent near-spinodal explosive boiling, which result in the acoustic pressure buildup and subsequent lift-off[18] of the droplets. Particularly, these calculations show that the near-spinodal temperatures $T_{max} \approx (6.2 \pm 0.8) \times 10^2$ K are achieved at the threshold fluence $F_B \approx 0.20 \pm 0.04$ J/cm^2 during the tail half of the excimer laser pulse at $\tau_{boil} \approx 30$–45 ns. These calculated temperatures are consistent with characteristic spinodal temperatures for water at positive pressures, $T_{spin}(P>0) \geqslant 0.92 T_{crit}$,[5] i.e., $T_{spin}(P>0) \geqslant 595$ K, and with the experimental value of 520 K,[17] obtained by extrapolation from optical transmission studies of explosive boiling of bulk water on an atomically smooth Si surface on a comparable timescale of 100–200 ns.

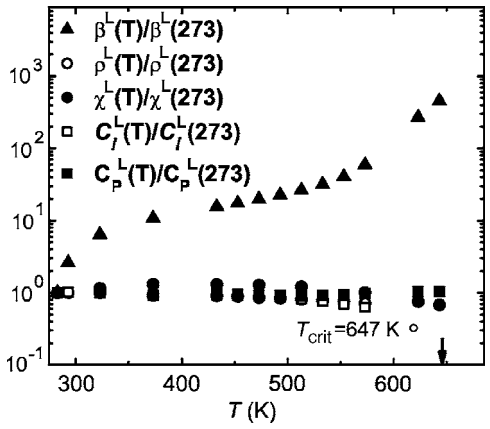

FIG. 10. Temperature dependences of normalized thermophysical parameters of water after (Refs. 5 and 32).

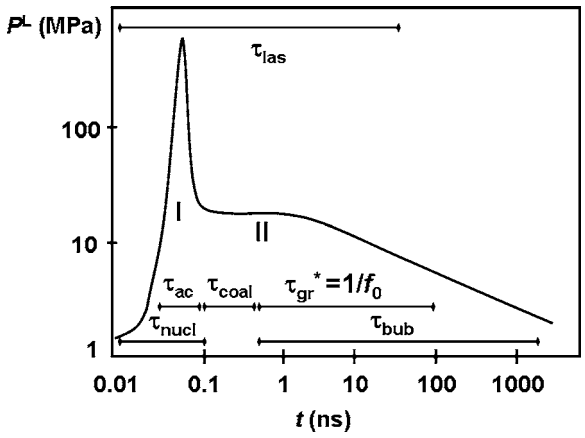

FIG. 11. Schematic of supposed acoustic pressure P^L transient and characteristic timescales for explosive boiling at laser-heated interfaces between water droplets and Si wafers. The following notations are used: τ_{las} for the laser pulse duration, τ_{nucl} for the nucleation time of nanobubbles, τ_{ac} for the acoustic relaxation time, τ_{coal} for the nanobubble coalescence time, τ_{bub} for the lifetime of microbubbles, and τ_{gr}^{*} for their growth time.

IV. DISCUSSION

The experimental and calculation results of this work can been interpreted assuming that several basic processes are involved in laser-induced removal (lift-off) of thin layers of low-boiling liquids (in a film or droplet form) from absorbing Si substrates. For our experimental conditions, the corresponding processes are: (1) fast (subnanosecond or even faster) buildup of a high pressure, P_{NL}, in a superheated interfacial water layer due to the strong thermoacoustic nonlinearity under near-critical conditions;[20,30] (2) fast (sub-nanosecond[20,21]) explosive nucleation and growth of interfacial nanometer-sized steam bubbles ("nucleate boiling"[4]) under the near-critical conditions during acoustic relaxation of P_{NL} via propagation of an acoustic wave in water microdroplets and in the underlying Si substrate and accompanying expansion of the superheated liquid layer; (3) fast (subnanosecond) avalanchelike coalescence of the nanobubbles to a single interfacial "flat" microbubble/steam layer (or several separate bubbles) in each water droplet building up again a high transient pressure inside the bubble(s) in such a "film boiling" regime; (4) submicrosecond growth of the interfacial microbubble from the Si surface driven by its internal vapor pressure with corresponding microflows in the top cooler liquid layer; and (5) final detachment of the entire droplet from the hosting surface at the certain lift-off velocity.

A. Near-critical buildup of pressure

According to the photoacoustic results of this work, at $F<F_B$, i.e., far from the liquid/vapor spinode curve and $T_{max}\leqslant 0.9T_{crit}$, the thermoacoustic pressure in the interfacial superheated water layer changes during the heating laser pulse for the acoustically free water/Si boundary as $P(t) \propto (dI_{las}/dt')_{t'=t}$,[30] representing a linear thermoacoustic response with a nanosecond acoustic relaxation time $\tau_{ac} \sim H/C_l^L$. However, at elevated temperatures ($T\geqslant 0.9T_{crit}$), corresponding to $F\geqslant F_B$, there are manifestations of a strong nearspinodal thermoacoustic nonlinearity, as the partial derivative of the liquid volume V^L with respect to its temperature $(\partial V^L/\partial T)_{Tspin}=\infty$ along the liquid/vapor spinode curve in the near-critical region[5] (Fig. 10) because of the intrinsic anharmonicity of van der Waals interparticle potentials and enhanced density fluctuations (nucleation of subcritical steam bubbles) at these elevated temperatures. Under these conditions, the subnanosecond rate of thermoacoustic pressure generation in the interfacial superheated water layers on the Si/water interface, $(\partial P^L/\partial t)_{gen} \approx K^L[(\partial V^L/\partial T)_P/V^L{}_0] \times (dT/dt)$ see notations below, may become comparable to the acoustic relaxation rate, $(\partial P^L/\partial t)_{relax}$, characterized by the nanosecond τ_{ac}. As a result, the originally free water/Si boundary becomes an impedance (confined) one, switching the acoustic generation regime and changing the shapes of the experimentally observed acoustic transients from the characteristic bipolar to monopolar ones [Fig. 4(b)]. Depending on the heating rate (dT/dt) of the interfacial water layer at $T\geqslant 0.9T_{crit}$ calculated using the SLIM software, the value of the resulting thermoacoustic pressure $P_{NL} \sim G(\partial P^L/\partial t)_{gen}\tau_{nucl}$ may approach 10^2 MPa (peak I in Fig. 11), according to the near-spinode molar volume change of fluids, $(\Delta V^L/V^L{}_0)_{Tspin}=[(V^L-V^L{}_0)/V^L{}_0]_{Tspin}\approx 1-2$ at $T \approx 590-647$ K {thermal expansion coefficient of water $\beta^L(T_{spin})=[(\partial V^L/\partial T)_P/V^L{}_0]_{Tspin} \sim 10^{-(1-2)}$ K^{-1} for the liquid volume at the binode $V^L{}_0$}, estimated from the van der Waals equation of state,[5] $(dT/dt) \sim 10^2$ K/ns (Fig. 6, inset) and the adiabatic bulk modulus of water, $K^L \approx 2\times 10^3$ MPa, estimated using the reported[32] values of the water mass density, $\rho^L(300\text{ K}) \approx 1\times 10^3$ kg/m^3, and its longitudinal speed of sound, $C_l^L(300\text{ K}) \approx 1.4\times 10^3$ m/s, under normal conditions. In these estimates the scaling factor G accounts for boiling kinetics (nucleation and growth of supercritical steam bubbles) effect on the quasistatic nonlinear thermoacoustic generation regime and equals to $G=[\chi^L\tau_{nucl}]^{1/2}/(C_l^L\tau_{nucl}) \sim 10^{-(1-2)}$ for $\chi^L \approx 1.5\times 10^{-3}$ cm^2/s (Ref. 32) and the characteristic nucleation time for critical bubbles τ_{nucl}, which is a strong function of pressure and temperature in the liquid and usually is not known exactly, varying from ~10 ps (Ref. 22 and 23) to 10^2 ps (Ref. 5, 34, and 35) or even several nanoseconds[5] as a function of degree of superheating.[23] Note that this described pressure buildup suppresses the near-

spinodal boiling process until acoustic relaxation of P_{NL}. The temperature rise in the superheated interfacial water layer, $\delta T \approx (dT/dt)\tau_{nucl}$, also strongly depends on the magnitude of τ_{nucl}, varying from a few K at $\tau_{nucl} \sim 10$ ps to a few tens of K at $\tau_{nucl} \sim 10^2$ ps (Ref. 34 and 35) for $(dT/dt) \sim 10^2$ K/ns, while the resulting maximum temperatures, $T_{max} \approx 0.9T_{crit} + \delta T$, have near-critical magnitudes. Our experimental results, particularly, saturation of $P^L(F)$ curve in Fig. 6 at $F > F_B$ may indicate that increase of δT is not very significant because of its self-limiting resulting from shorter τ_{nucl} at higher temperatures.[23]

B. Explosive nucleation of nanobubbles

For $P_{NL} \sim 10^2$ MPa, which is much higher than the critical pressure of water, $P_{crit}=22.4$ MPa,[32] and $T_{max} \leqslant T_{crit}$, the thin interfacial water layers on the Si substrates are not superheated and density fluctuations representing subcritical steam bubbles are not stable. However, these layers become superheated again during relaxation of the thermoacoustic pressure P_{NL} on a subnanosecond time scale, starting at the time during the heating laser pulse, when $(\partial P^L/\partial t)_{gen}$ becomes smaller than $(\partial P^L/\partial t)_{relax}$ and the transient P^L magnitude falls below the saturated water vapor pressure, P_{sat}, at the water/Si interface for the corresponding liquid temperatures $T_{spon} \leqslant T_{crit}$. The interface energy density taken away by the released acoustic wave can be estimated in a plane-wave approximation as

$$\Phi = \frac{\int_0^{Ldep} {P_{NL}}^2 dz}{2\rho^L C_l^{L^2}}, \tag{1}$$

showing that for the above mentioned values of parameters ρ^L, C_l^L, and P_{NL} the mechanical energy density Φ in the interfacial superheated water layers of effective thickness $L_{dep} \approx [\chi^L \tau_{nucl}]^{1/2} \approx 1-4$ nm for $\chi^L \approx 1.5 \times 10^{-3}$ cm^2/s (Ref. 32) and $\tau_{nucl} \sim 10-10^2$ ps may approach 0.02 J/cm^2, i.e., about 10% of F_B in qualitative agreement with literature results.[36] This effect and the resulting thermal expansion of the layers are accompanied by their cooling to subcritical temperatures $T_{spon} < T_{crit}$. The temperature and effective thickness L_{dep} of the superheated water layer, corresponding to the maximum radius of critical bubbles $r \sim L_{dep}/2 \sim 1$ nm, dictate a magnitude of a liquid pressure P_{nucl}^L, which, according to the metastable equilibrium condition,[5] allows nucleation of critical steam bubbles

$$P_{nucl}^L \leqslant P_{sat}(T_{spon}) - \frac{2\delta\gamma(T_{spon}, r)}{r[1 - V^L(T_{spon})/V^V(T_{spon})]}, \tag{2}$$

where V^V is the molar volume of water vapor at T_{spon} ($V^V \gg V^L$ outside of the critical point), $\gamma(T,r)$ is the temperature- and size-dependent surface tension of water, and the positive value $\delta \leqslant 1$ is an accommodation coefficient accounting for hemispherical shape of steam bubbles nucleating on a smooth Si surface. Typical values of thermal parameters of water—$P_{sat} \sim 10$ MPa $\leqslant P_{crit}$ and $\gamma \sim 1-10$ mN/m (Ref. 5) give for P_{nucl}^L values increasing from -10 MPa at $T_{spon} \approx 0.9T_{crit}$ to P_{crit} at $T_{spon} \approx T_{crit}$. Finally, such nucleation of critical vapor bubbles becomes a steady-state process after the pressure- and temperature-dependent induction time τ_{nucl}.

Even though, strictly speaking, the steam bubble nucleation on Si surfaces is a heterogeneous process, for the atomically smooth surfaces of Si wafers[17] and the high degrees of superheating[5] for water the "threshold" temperature for subnanosecond explosive boiling can be shown to correspond to its near-spinodal temperatures, i.e., the explosive boiling process exhibits a homogeneous character with the only heterogeneous feature the hemispherical shape of the resulting steam bubbles. Assuming that the nanometer-sized vapor bubbles almost completely fill the entire nanometer-thick superheated interfacial water layer during $\tau_{nucl} \sim 10-10^2$ ps, the steady-state bubble nucleation rate, $J \sim 1/[(2r)^3 \tau_{nucl}]$, can be estimated for a smooth Si surface. This rate, $J \sim 10^{30-31}$ cm^{-3} s^{-1}, is quite close to the asymptotic nucleation rate, $J_{max} \sim 10^{32}$ cm^{-3} s^{-1}, near the liquid/vapor spinode curve at $r=0$ and correspond, according to published data,[5] to T_{spon} values in the narrow range near the liquid/vapor spinode curve of water at positive external pressures, where fast homogeneous nucleation takes place. Moreover, one can consider steady-state heterogeneous nucleation on a smooth surface[5]

$$J_{het} = N^{2/3} \frac{1+\cos\varphi}{2} \sqrt{\frac{6\gamma}{(2+P_{liq}/P_{sat})\pi m h(\varphi)}} \times \exp\left[-\frac{16\pi\gamma^3 h(\varphi)}{3k_B T(P_{sat}-P_{liq})^2(1-V^L/V^V)^2}\right], \tag{3}$$

where N, φ, m, and k_B are the density of molecules in liquid water, contact angle for water on a Si surface with a native oxide layer, water molecular mass, temperature- and size-dependent water surface tension, and Boltzmann constant, respectively. Also, in this equation P_{liq} is the static or transient pressure in the host liquid ($P_{liq}=P^L$ for $P^L \leqslant P_{sat}$), while $h(\varphi)=0.25(1+\cos\varphi)^2(2-\cos\varphi)$ is the geometric correction factor to the work of interfacial critical bubble formation, given in the square brackets of Eq. (3). Near the spinode curve of superheated water the contact angle for water on a Si surface tends to zero, following the similar trend for γ,[5] and the latter equation transforms to that for homogeneous bubble nucleation at $h(\varphi)=1$.

It is useful also to estimate a growth time, τ_{gr}, for the nanobubbles nucleating in the interfacial superheated water layers under the near-spinode conditions and "blown up" by P_{NL}. It can be estimated using the Rayleigh equation[4] adapted to the form $P_{NL} \approx 0.9\rho^L(r/\tau_{gr})^2$. For $P_{NL} \sim 10^2$ MPa, $\rho^L(300\text{ K}) \approx 1 \times 10^3$ kg/m^3, and $r \sim 1$ nm, the minimal $\tau_{gr} \sim 10$ ps, which is consistent with characteristic $\tau_{nucl} \sim 10$ ps.[1,2,22,23,34,35]

C. Coalescence of nanobubbles and release of "hidden" pressure

It is thermodynamically advantageous for steam nanobubbles closely packed in the interfacial water layers at temperature $T_{spon} \geqslant 0.9T_{crit}$ and pressure $P_{spin}(T_{spon})$ to merge together within the layers, converting their surface energy to additional (noncompensated) vapor pressure, which "blows

up" the coalesced nanobubbles to larger dimensions and permanently increases during the "avalanche" coalescence process. The reason is that after the near-spinode quasihomogeneous nucleation of steam nanobubbles at the hot Si substrate, a significant part of their internal vapor pressure P_{sat} is hidden, working to stabilize the bubbles against the surface tension force [see Eq. (2)]. Therefore, when these nanobubbles coalesce in the interfacial superheated water layer to give a flat vapor bubble (film) representing a "macroscopic" vapor phase, the hidden vapor pressure $P_{hid}(T_{spon}) \approx [P_{sat}(T_{spon}) - P_{spin}(T_{spon})]$ is released, driving growth of the resulting microbubble over the time $\tau_{gr}^* \sim 1/f_0 \approx 10^2$ ns.[21] The maximum P_{hid} can be released during steam nanobubble coalescence at $T_{spon} \approx 0.95 T_{crit} \approx 620$ K, when $P_{spin}(T_{spon}) \approx 0$ and $P_{sat}(620\ \text{K}) \approx 16$ MPa;[5] in contrast, at the critical point of water, where the liquid/vapor binode and spinode curves merge together,[5] $P_{hid} \approx 0$.

The estimated maximum value of the released hidden pressure—$P_{sat}(0.95T_{crit})$—is consistent with P^L magnitudes measured in this and previous work.[20] According to our previous results,[20] for $F < F_B$ at moderate water/Si interface temperatures far from T_{crit}, acoustic generation at the interface is expected to occur in the "free boundary" mode and the corresponding water (P_f^L) and Si (P_f^S) acoustic responses are linear thermoacoustic. One can estimate that $P_f^S \approx \sigma^S L_{dep}{}^S/(C_l^S \tau_{las}) \approx 0.6$ MPa for $T \approx 580\ \text{K} < T_{crit}$, the volume thermal expansion coefficient of Si $\beta^S(580\ \text{K}) \approx 3.5 \times 10^{-6}\ \text{K}^{-1}$ and its bulk adiabatic modulus $K_{ad}{}^S(580\ \text{K}) \approx 1 \times 10^{11}$ Pa,[32] the energy deposition depth in Si $L_{dep}{}^S \approx [\chi^S \tau_{las}]^{1/2} \approx 0.7$ μm calculated with the computer code SLIM (see details of these calculations above), the longitudinal speed of sound in Si $C_l^S \approx 8.4 \times 10^3$ m/s (Ref. 32) and $\tau_{las} \approx 20$ ns, taking the thermoacoustic stress in Si in the form $\sigma^S(T) \approx [K_{ad}{}^S(T)\beta^S(T)](T-300)$. In agreement with experimental results in Fig. 5, showing $P_S^f > P_L^f$ at $F < F_B$, the estimated linear thermoacoustic water response, $P_f^L \sim \sigma^L(T) L_{dep}{}^L/(C_l^S \tau_{las})$, is considerably smaller—about 0.3 MPa—for the thermoacoustic stress in water $\sigma^L(T) \approx [\rho^L(T) C_l^L(T)^2 \beta^L(T)](T-300)$, the volume thermal expansion coefficient of water $\beta^L(573\ \text{K}) \approx 4.2 \times 10^{-3}\ \text{K}^{-1}$,[5] the water mass density $\rho^L(573\ \text{K}) \approx 7 \times 10^2\ \text{kg/m}^3$,[5] the water longitudinal speed of sound $C_l^L(573\ \text{K}) \approx 9 \times 10^2$ m/s,[5] and the energy deposition depth in water $L_{dep}{}^L \approx [\chi^L(T)\tau_{las}]^{1/2} \approx 0.05$ μm estimated for $\chi^L(T) \approx 1.5 \times 10^{-3}\ \text{cm}^2/\text{s}$.[32] In contrast, in Fig. 6 for $F > F_B$ the saturated P^L values are more than an order of magnitude (about 15 times) higher than at $F \leqslant F_B$ and can be estimated as $15(P_f^S + P_f^L) \approx 14$ MPa, which is close to $P_{sat}(620\ \text{K}) \approx 16$ MPa.[5]

This analysis may mean that the acoustic response P^L measured in this study for wet Si surfaces at $F > F_B$ represents the only released hidden pressure $P_{hid}(T_{spon}) \sim 1-10$ MPa (stage II in Fig. 11) and does not include the preceding more intense and faster component P_{NL}. This assumption is consistent with results of other studies,[20] where a two-pulse structure of "wet" acoustic responses has been considered. Technically, only the second, relatively long ($t \sim \tau_{gr}^* \sim 1/f_0 \approx 10^2$ ns)[21] and low-amplitude ($P_{hid} \sim 1-10$ MPa $\leqslant P_{crit}$) pulse of such acoustic transients can be currently detected by present photoacoustic, photodeflection and surface-plasmon probe techniques,[14,15,20] while the first, ultrafast ($t \sim \tau_{nucl} \sim 10-10^2$ ps)[22,23,34,35] and high-amplitude [$P_{NL} \sim 10^2$ MPa (Ref. 20)] pulse is subject to a strong diffraction effect and, even more important, to strong frequency-dependent dissipative losses in liquid[14] and/or in protective cases of acoustic transducers during its propagation to the actual detection region. For example, the estimated ultrasound penetration depth, $\alpha_{ac}{}^{-1}$, in water is about 40 μm at $f \approx 1$ GHz and 0.4 μm at $f \approx 10$ GHz for the nonlinear attenuation coefficient $\alpha_{ac}/f^2 \approx 25 \times 10^{-15}\ \text{s}^2\ \text{m}^{-1}$,[14,32] while in brass $\alpha_{ac}{}^{-1} \sim 10^2$ μm at $f \approx 1$ GHz and 10 μm at $f \approx 10$ GHz for the linear attenuation coefficient $\alpha_{ac}/f \approx 7 \times 10^{-6}\ \text{sm}^{-1}$.[32] Moreover, it was concluded in other previous studies[20] that explosive boiling pressure driving lift-off of micron-thick water droplets or entire IPA layers at velocities of a few tens of m/s should be close to 1 GPa, i.e., on the order of P_{NL}.

Although the $P^L(F)$ curve in Fig. 6 has a similar shape (the steep thresholdlike rise followed by a "plateau") as the fluence dependence of the compressive pressure reported earlier for explosive boiling at bulk water/metal film interfaces,[14,15] the experimentally measured compressive pressure values on the corresponding plateaus in those works were considerably lower—1–3 MPa,[14,15] as well as the measured boiling temperatures $T_{spon} \approx 400-500$ K of water.[9,10] The most probable reason for this discrepancy between results of our and those studies is the rough surfaces of the Ag or Cr metallic substrates used in the cited works. Substrate surface roughness has a strong effect on laser-induced surface boiling of water as was demonstrated for rough and smooth Si substrates exhibiting for water $T_{spon} \approx 430$ and 520 K, respectively.[17]

Finally, a characteristic "avalanche" coalescence time, τ_{coal}, for the densely packed steam nano bubbles driven by $P_{hid} \sim 1-10$ MPa was estimated. Using a viscous flow equation $P = \eta(dv/dz)$ for the Stokes regime[37] in the form $P_{hid} \approx \eta(T_{spon})(r/\tau_{coal})/r$, one obtains a rough estimate for $\tau_{coal} \sim 10$ ps at the characteristic water viscosity $\eta(T) \approx 10^{-4}$ Pa s.[32] The same estimate for τ_{coal} is obtained for the Knudsen flow regime,[37] when $P_{hid} \approx \rho^L(r/\tau_{coal})^2$, for $\rho^L(300\ \text{K}) \approx 1 \times 10^3\ \text{kg/m}^3$ and $r \sim 1$ nm. Experimental τ_{coal} values in superheated liquids are close to 0.5 ns,[21,35] indicating much slower (nonavalanche) coalescence process. Because of the short (subnanosecond) coalescence dynamics, features related to nanobubble oscillations are absent in our acoustic transients in Figs. 4 and 7.

D. Dynamics of microbubbles and lift-off of water droplets

The flat interfacial steam bubble formed by coalesced nanobubbles grows to a hemispherical shape and then oscillates at a frequency $f_0 \approx U_{max}/R_{max}$, where $U = dR/dt$ is the growth rate of a bubble with maximum radius $R = R_{max}$. According to the Rayleigh equation,[4] $P_{hid} \approx 0.91 \rho^L U_{max}{}^2$, the growth rate is estimated to be $U \sim 10-10^2$ m/s (Refs. 1 and 2) for $P_{hid} \sim 1-10$ MPa, $\rho^L(300\ \text{K}) \approx 1 \times 10^3\ \text{kg/m}^3$, and $f_0 \approx 10$ MHz. This rate exceeds many times the experimentally measured bubble growth rates of 1–3.6 m/s during hetero-

geneous boiling of water on laser-heated rough metal surfaces,[10,12,15] while it is in agreement with large bubble growth rates $U_{max} \sim 10^2$ m/s during explosive boiling experiments in bulk absorbing liquids.[26] Moreover, under our experimental conditions R_{max} can approach 10 μm, becoming comparable to the water droplet's height $H \approx 7-10$ μm (Fig. 1) and contributing to final detachment of these water droplets from the Si substrate.

The main factors determining characteristics of the lift-off process of a thin transparent liquid layer from a hot absorbing solid substrate have been deduced in previous studies.[18–20] First, there is a degree of superheating of an interfacial liquid layer, $\Delta T = T - T_{spon}(P=1 \text{ atm})$, resulting in its strong thermal expansion and high compressive stress in the entire liquid layer. Second, the thickness of the superheated liquid layer, L_{dep}, affects the potential elastic energy of the cooler liquid layer. Finally, the thickness of the entire liquid layer or liquid droplets determines the onset of lift-off and the corresponding lift-off velocity u_{lift}. Moreover, one can associate the microsecond lifetimes of microbubbles, $\tau_{bub} \sim 1$ μs, measured in this work with lift-off times for water micro-droplets containing these bubbles. Then, u_{lift} may approach $H/\tau_{bub} \sim 10$ m/s, consistent with characteristic water plume velocities (about 10 m/s) measured under similar experimental conditions,[18,19,21] or estimated using the formula $u_{lift} \approx C_l^L (\Delta V^L / V_0^L)_{Tspin} L_{dep}/H$ (Ref. 19) and the above-mentioned input parameters.

V. CONCLUSIONS

In conclusion, we report a contact photoacoustic study of explosive boiling and lift-off of a predeposited layer of transparent micron-sized water droplets from an absorbing Si wafer heated by a nanosecond KrF laser with recording of acoustic transients on the rear side of the Si wafer. The rapid increase of the acoustic response at a threshold laser fluence, F_B, of 0.20 J/cm^2 and its subsequent leveling off at a value on the order of the water critical pressure in the fluence range of 0.2–0.4 J/cm^2 are attributed to explosive boiling of superheated water driven by the strong nonlinearity of the water thermal expansion coefficient near the liquid-vapor spinode curve. Under these experimental conditions, the recorded acoustic transients contained several characteristic multi-megahertz contributions from spatially separated micron-sized steam bubbles with microsecond lifetimes nucleated in separate micron-sized water droplets. These studies give an insight into microscopic mechanisms and basic parameters of thresholdlike fast buildup of acoustic pressure, explosive nucleation of interfacial steam nanobubbles, and their coalescence to microbubbles in the host water droplets, growth of these microbubbles followed by lift-off of the droplets. Also, these studies provide more detailed understanding of basic mechanisms of related phenomena such as steam laser cleaning[2] and laser-induced forward transfer,[3] widely used in similar experimental geometries.

ACKNOWLEDGMENTS

The authors gratefully acknowledge funding of this work by National Science Foundation (Grant No. 0218024) and technical support of these experiments by Professor Alexander A. Karabutov and Shishir Shukla.

[1] H. C. Lee, B. D. Oh, S. W. Bae, M. H. Kim, J. Y. Lee, and I. S. Song, J. Nucl. Sci. Technol. **40**, 768 (2003).
[2] F. Lang, M. Mosbacher, and P. Leiderer, Appl. Phys. A: Mater. Sci. Process. **77**, 117 (2003); S. I. Kudryashov and S. D. Allen, Proc. SPIE **5713**, 528 (2005).
[3] A. Morimoto, H. Tanimura, H. Yang, S. Otsubo, M. Kumeda, and X. Chen, Appl. Phys. A: Mater. Sci. Process. **79**, 1015 (2004).
[4] S. van Stralen and R. Cole, *Boiling Phenomena: Physicochemical and Engineering Fundamentals and Applications* (Hemisphere, Washington, 1979), Vols. 1 and 2.
[5] V. P. Skripov, E. N. Sinitsyn, P. A. Pavlov, G. V. Ermakov, G. N. Muratov, N. V. Bulanov, and V. G. Baidakov, *Thermophysical Properties of Liquids in the Metastable State* (Gordon and Breach, New York, 1988).
[6] K. P. Weninger, H. Cho, R. A. Hiller, S. J. Putterman, and G. A. Williams, Phys. Rev. E **56**, 6745 (1997); for bibliography see also M. P. Brenner, S. Hilgenfeldt, and D. Lohse, Rev. Mod. Phys. **74**, 425 (2002).
[7] J. Holzfuss, M. Rüggeberg, and A. Billo, Phys. Rev. Lett. **81**, 5434 (1998); Z. Q. Wang, R. Pecha, B. Gompf, and W. Eisenmenger, Phys. Rev. E **59**, 1777 (1999); R. Pecha and B. Gompf, Phys. Rev. Lett. **84**, 1328 (2000).
[8] D. H. Trevena, *Cavitation and Tension in Liquids* (Hilger, Bristol, 1987).
[9] H. K. Park, C. P. Grigoropoulos, C. C. Poon, and A. C. Tam, Appl. Phys. Lett. **68**, 596 (1996).
[10] O. Yavas, P. Leiderer, H. K. Park, C. P. Grigoropoulos, C. C. Poon, W. P. Leung, N. Do, and A. C. Tam, Phys. Rev. Lett. **70**, 1830 (1993).
[11] P. T. Leung, N. Do, L. Klees, W. P. Leung, F. Tong, L. Lam, W. Zapka, and A. C. Tam, J. Appl. Phys. **72**, 2256 (1992).
[12] D. Kim, H. K. Park, and C. P. Grigoropoulos, Int. J. Heat Mass Transfer **44**, 3843 (2001); D. Kim and J. Lee, J. Appl. Phys. **93**, 762 (2003).
[13] N. Do, L. Klees, A. C. Tam, P. T. Leung, and W. P. Leung, J. Appl. Phys. **74**, 1534 (1993).
[14] H. K. Park, D. Kim, C. P. Grigoropoulos, and A. C. Tam, J. Appl. Phys. **80**, 4072 (1996).
[15] O. Yavas, A. Schilling, J. Bischof, J. Boneberg, and P. Leiderer, Appl. Phys. A: Mater. Sci. Process. **64**, 331 (1997).
[16] K. F. MacDonald, V. A. Fedotov, S. Pochon, B. F. Soares, N. I. Zheludev, C. Guignard, A. Mihaescu, and P. Besnard, Phys. Rev. E **68**, 027301 (2003).
[17] M. Mosbacher, M. Bertsch, H.-J. Münzer, V. Dobler, B.-U. Runge, D. Bäuerle, J. Boneberg, and P. Leiderer, Proc. SPIE **4426**, 308 (2002).
[18] S. I. Kudryashov and S. D. Allen, J. Appl. Phys. **93**, 4306 (2003).
[19] S. I. Kudryashov and S. D. Allen, Appl. Phys. A: Mater. Sci. Process. **79**, 1737 (2004).
[20] S. I. Kudryashov and S. D. Allen, J. Appl. Phys. **95**, 5820 (2004).
[21] F. Lang and P. Leiderer, New J. Phys. **8**, 14 (2006); see also F. Lang, P. Leiderer, and S. Georgiou, Appl. Phys. Lett. **85**, 2759 (2004).
[22] Y. Dou, L. V. Zhigilei, N. Winograd, and B. J. Garrison, J. Phys. Chem. **105**, 2748 (2001).
[23] B. Garrison, T. E. Itina, and L. V. Zhigilei, Phys. Rev. E **68**, 041501 (2003).
[24] K. Hatanaka, M. Kawao, Y. Tsuboi, H. Fukumura, and H. Masuhara, J. Appl. Phys. **82**, 5799 (1997); D. Kim and C. P. Grigoropoulos, Appl. Surf. Sci. **127–129**, 53 (1998); I. Apitz and A. Vogel, Proc. SPIE **4961**, 48 (2003).
[25] V. Kotaidis and A. Plech, Appl. Phys. Lett. **87**, 231102 (2005).
[26] S. I. Kudryashov, K. Lyon, and S. D. Allen, Appl. Phys. Lett. **88**, 214105 (2006); Phys. Rev. E **73**, 055301 (2006).
[27] W. H. Lawnik, U. D. Goepel, A. K. Klauk, and G. H. Findenegg, Langmuir **11**, 3075 (1995).
[28] S. I. Kudryashov and S. D. Allen, J. Appl. Phys. **92**, 5627 (2002).
[29] *Handbook of Optical Constants of Solids*, edited by E. D. Palik (Academic, Orlando, 1985).
[30] V. E. Gusev and A. A. Karabutov, *Laser Optoacoustics* (AIP, New York, 1993), Chaps. 2, 4, and 7.
[31] V. A. Shutilov, *Fundamental Physics of Ultrasound* (Gordon and Breach, New York, 1988).
[32] I. S. Grigor'ev and E. Z. Meilikhov, *Fizicheskie Velichini* (*Physical Quantities*, Energoatomizdat, Moscow, 1991) (in Russian).
[33] R. Singh and J. Viatella, computer code SLIM (University of Florida, 1991, 1992).

[34]F. F. Abraham, D. E. Schreiber, M. R. Mruzik, and G. M. Pound, Phys. Rev. Lett. **36**, 261 (1976).
[35]Values of $\tau_{\mathrm{nucl}} \approx 10^2$ ps and $\tau_{\mathrm{coal}} \approx (5-6) \times 10^2$ ps can be obtained using data in Fig. 4 in Ref. 21.
[36]A. Vogel, J. Noack, G. Hüttman, and G. Paltauf, Appl. Phys. B: Lasers Opt. **81**, 1015 (2005).
[37]S. P. Kiselev, E. V. Vorozhtsov, and V. M. Fomin, *Foundations of Fluid Mechanics with Applications* (Birkhäuser, Boston, 1999).